Heat and Mass Transfer 38 (2001) 55–63 © Springer-Verlag 2001

# A numerical study of effects of the swinging amplitude of fins on heat transfer characteristics in a flow

**W.-S. Fu, S.-J. Yang**



**Abstract** A new method for enhancing heat transfer of a finned heat sink is proposed in this study. In this method, extremely thin fins are installed in the finned heat sink, and these fins may swing back and forth in a flow because of the fluid flowing pass them. As a result, the velocity and thermal boundary layers attached on the fins are then contracted and disturbed, and the heat transfer rate of the fins can be enhanced. The variations between the fluid and fins are dynamic and belong to a kind of the moving boundary problems. The arbitrary Lagrangian–Eulerian (ALE) kinematic description method is available and adopted to describe the flow and thermal fields, and the governing equations are solved using the Galerkin finite element method with moving meshes. The effects of variations in the Reynolds number, swinging speed and amplitude of the fins on the heat transfer of the fins are investigated. The results show that the velocity and thermal boundary layers may be contracted and disturbed as the fins swing with a large speed, and the heat transfer rates are remarkably affected by the swinging speed and amplitude of the fins.

**List of symbols**

| | |
|---|---|
| $a$ | dimensional amplitude of the fins, m |
| $A$ | dimensionless amplitude of the fins ($A = a/w_2$) |
| $d$ | dimensional thickness of the fins, m |
| $D$ | dimensionless thickness of the fins ($D = d/w_2$) |
| $h$ | dimensional width of the channel, m |
| $H$ | dimensionless width of the channel ($H = h/w_2$) |
| $h_1$ | dimensional distance from the wall of the channel to the fin, m |
| $H_1$ | dimensionless distance from the wall of the channel to the fin ($H_1 = h_1/w_2$) |
| $h_2$ | dimensional pitch of the fins, m |
| $H_2$ | dimensionless pitch of the fins ($H_2 = h_2/w_2$) |
| $\mathrm{Nu}$ | overall average Nusselt number of the fin |
| $\overline{\mathrm{Nu}}$ | time-average overall Nusselt number of the fin |
| $\mathrm{Nu}_X$ | local Nusselt number on the top or bottom surface of the fin |
| $\overline{\mathrm{Nu}_X}$ | average Nusselt number on the top or bottom surface of the fin |
| $p$ | dimensional pressure, $\mathrm{N}\cdot\mathrm{m}^{-2}$ |
| $p_\infty$ | referential pressure, $\mathrm{N}\cdot\mathrm{m}^{-2}$ |
| $P$ | dimensionless pressure ($P = (p - p_\infty)/\rho u_0^2$) |
| Pr | Prandtl number ($\mathrm{Pr} = \alpha/\nu$) |
| Re | Reynolds number ($\mathrm{Re} = u_0 w_2/\nu$) |
| $\mathrm{Re}_\iota$ | Reynolds number for the Blasius solution ($\mathrm{Re}_\iota = u_0\iota/\nu$) |
| $s_\mathrm{f}$ | dimensional swinging speed of the fins, $\mathrm{m}\cdot\mathrm{s}^{-1}$ |
| $S_\mathrm{f}$ | dimensionless swinging speed of the fins ($S_\mathrm{f} = s_\mathrm{f}/u_0$) |
| $t$ | dimensional time, s |
| $T$ | dimensional temperature, °C |
| $T_\mathrm{f}$ | dimensional temperature of the fin, °C |
| $T_0$ | dimensional temperature of the inlet fluids, °C |
| $u, v$ | dimensional velocities in $x$ and $y$ directions, $\mathrm{m}\cdot\mathrm{s}^{-1}$ |
| $U, V$ | dimensionless velocities in $X$ and $Y$ directions ($U = u/u_0,\ V = v/u_0$) |
| $u_0$ | dimensional velocity of the inlet fluids, $\mathrm{m}\cdot\mathrm{s}^{-1}$ |
| $v_\mathrm{f}$ | dimensional swinging velocity of the fin in $y$-direction, $\mathrm{m}\cdot\mathrm{s}^{-1}$ |
| $V_\mathrm{f}$ | dimensionless swinging velocity of the fin in $Y$-direction ($V_\mathrm{f} = v_\mathrm{f}/u_0$) |
| $\hat{v}$ | dimensional mesh velocity in $y$-direction, $\mathrm{m}\cdot\mathrm{s}^{-1}$ |
| $\hat{V}$ | dimensionless mesh velocity in $Y$-direction, ($\hat{V} = \hat{v}/u_0$) |
| $w$ | dimensional length of the channel, m |
| $W$ | dimensionless length of the channel ($W = w/w_2$) |
| $w_1$ | dimensional distance from the inlet to the front side of the fin, m |
| $W_1$ | dimensionless distance from the inlet to the front side of the fin ($W_1 = w_1/w_2$) |
| $w_2$ | dimensional length of the fin, m |
| $W_2$ | dimensionless length of the fin ($W_2 = w_2/w_2$) |
| $x, y$ | dimensional Cartesian coordinates, m |
| $X, Y$ | dimensionless Cartesian coordinates ($X = x/w_2$, $Y = y/w_2$) |

**Greek symbols**

| | |
|---|---|
| $\alpha$ | thermal diffusivity, $\mathrm{m}^2\cdot\mathrm{s}^{-1}$ |
| $\phi$ | computational variables |
| $\iota$ | the length of a flat plate for the Blasius solution, m |
| $\lambda$ | penalty parameter |
| $\nu$ | kinematic viscosity, $\mathrm{m}^2\cdot\mathrm{s}^{-1}$ |
| $\theta$ | dimensionless temperature ($\theta = (T - T_0)/(T_\mathrm{f} - T_0)$) |
| $\rho$ | density, $\mathrm{kg}\cdot\mathrm{m}^{-3}$ |

*Received on 25 April 2000*

W.-S. Fu (✉), S.-J. Yang
Department of Mechanical Engineering
National Chiao Tung University, 1001 Ta Hsueh Road
Hsinchu 30056, Taiwan, R.O.C.

The support of this work by the National Science Council of Taiwan, R.O.C., under contract NSC89–2212-E-009–010 is gratefully acknowledged.

$\tau$ dimensionless time ($\tau = tu_0/w_2$)
$\tau_p$ dimensionless time of one cycle
$\Delta\tau$ dimensionless time increment

**Other**
| | absolute value

## 1 Introduction



Due to the progress of the semiconductor technology, a trend of development of a new electronic device is focused on the miniaturization of components and compact packaging, which results in the larger heat being generated by the device and the junction temperature of the device being higher. The failure rate of an electron device had been statistically corrected to be proportional to the exponential of the device junction temperature. Thus the thermal problem has become an important issue for the performance and reliability of the electronic device. How to improve the thermal design and enhance the heat transfer rate for the electronic device becomes a very important subject.

The techniques for enhancing the heat transfer of electronic systems and devices have received much attention. Several models for the cooling of electronic components have been widely studied both numerically and experimentally. Incropera [1] reported the convection heat transfer methods in electronic equipment cooling. Yeh [2] summarized and reviewed the results of recent developments and researches of the heat transfer technologies in electronic devices, such as air cooling, liquid cooling, jet impingement, heat pipe, and micro-channel cooling. Sathe and Sammakia [3] made a survey of recent developments in detail for air cooling method in electronic equipment.

Adding a finned heat sink to a hot electronic device for enlarging the heat transfer area to enhance thermal performance is commonly employed in the electronic device. Several papers [4–6] were available in this area. Moreover, vibrating a heated body surface had been conducted experimentally and theoretically [7–10], that could increase the heat transfer rate remarkably.

However, at present, it appears that the efficiency of the heat transfer of adding the finned heat sink to the hot electronic device may fail to catch up with the large heat generation rate of the new electronic device. As for the vibration of the heated body surface, it will seriously reduce the reliability and life of the electronic device.

In this work, a new cooling model, which combines the finned heat sink and the vibration of heated body surface methods, is presented to enhance the heat transfer of the electronic device effectively and reliably. In this method, the finned heat sink is mounted on the surface of the electronic device. The fins of the finned heat sink may swing back and forth in a flow, but the device is stationary. To realize this concept, the fins are needed to be made of extremely thin metal, then these thin fins could easily swing back and forth in the flowing fluid, or these fins are forced to be oscillated by an artificial method, such as an oscillation exciter installed at a proper place. As this apparatus is executed, the boundary layers of the velocity and temperature attached on the fins may be disturbed and contracted due to the swinging of the fins, which can enhance the heat transfer rate.

Since the swinging fins interact with the flow, the variations of the flow and thermal fields become time-dependent and belong to a class of the moving boundary problems. To analyze this problem, the moving interfaces between the fluid and fins have to be considered. Thus, this problem is hardly analyzed by either the Lagrangian or Eulerian kinematic description method solely. An arbitrary Lagrangian–Eulerian (ALE) kinematic description method [11–14], which combine the characteristics of the Lagrangian and Eulerian kinematic description methods, is an appropriate method to describe this problem. In the ALE method, the computational meshes may move with the fluid (Lagrangian), be held fixed (Eulerian), or be moved in any other prescribed way. The detail of the kinematic theory of the ALE kinematic description method is delineated in [11, 12].

Therefore, the ALE description method is adopted to describe the variations of the flow and thermal fields induced by the interaction between the swinging fins and flowing fluid numerically. A Galerkin finite element method with moving meshes and a backward difference scheme, dealing with the time terms, are applied to solve the governing equations. The effects of variations in the Reynolds number, swinging speed and amplitude of the fins on the heat transfer of the fins are investigated.

## 2 Physical model

The physical model is shown in Fig. 1. There is a two-dimensional horizontal channel with width $h$ and length $w$. A finned heat sink with three thin fins is set in the channel. The fins with thickness $h_3$ and length $w_2$ are arranged with a pitch of $h_2$. The ratio of $h_3$ to $w_2$ is 0.01. The distances from the inlet and wall of the channel to the fins are $w_1$ and $h_1$, respectively. The inlet velocity $u_0$ and temperature $T_0$ of the fluid are uniform. These fins are made of high conductivity material and maintained at a constant temperature $T_f$, which is higher than $T_0$. Initially ($t = 0$), these thin fins are assumed to be stationary and the fluid flows steadily. As the time $t > 0$, these thin fins are swung back and forth induced by the flow (the photographs of the swinging fin are given in the Appendix). Then, the variations of the flow and thermal fields become time-dependent and are classified into a kind of the moving boundary problems. As a result, the ALE method is properly utilized to analyze this problem.

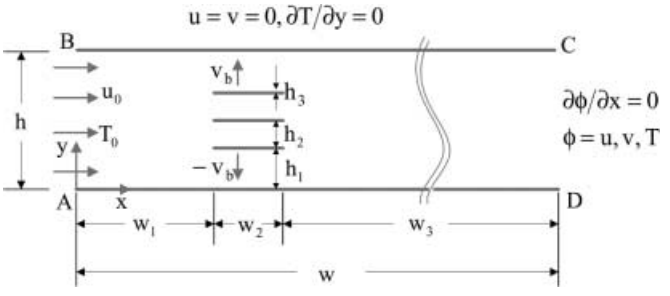


**Fig. 1.** Physical model

For facilitating the analysis, the following assumptions are made:

1. The fluid is air and the flow field is two-dimensional, incompressible and laminar.
2. The fluid properties are constant and the effect of the gravity is neglected.
3. The moving direction of the fins is in the $y$-direction only, and the fins swing with a constant swinging speed $s_f$.
4. The no-slip condition is held on the interfaces between the fluid and fins.

Based upon the characteristic scales of $w_2$, $u_0$, $\rho u_0^2$ and $T_0$, the dimensionless variables are defined as follows:

$$X=\frac{x}{w_2},\quad Y=\frac{y}{w_2},\quad U=\frac{u}{u_0},\quad V=\frac{v}{u_0},$$
$$\hat{V}=\frac{\hat{v}}{u_0},\quad V_f=\frac{v_f}{u_0},\quad S_f=\frac{s_f}{u_0},\quad P=\frac{p-p_\infty}{\rho u_0^2},$$
$$\tau=\frac{tu_0}{w_2},\quad \theta=\frac{T-T_0}{T_f-T_0},\quad \mathrm{Re}=\frac{u_0 w_2}{\nu},\quad \mathrm{Pr}=\frac{\nu}{\alpha}\ , \tag{1}$$

where $\hat{v}$ is the mesh velocity, $v_f$ and $s_f$ $(=|v_f|)$ are the swinging velocity and speed of the fins, respectively.

According to the above assumptions and dimensionless variables, the dimensionless ALE governing equations [11–14] are expressed as the following equations:

Continuity equation

$$\frac{\partial U}{\partial X}+\frac{\partial V}{\partial Y}=0\ , \tag{2}$$

Momentum equations

$$\frac{\partial U}{\partial \tau}+U\frac{\partial U}{\partial X}+(V-\hat{V})\frac{\partial U}{\partial Y}=-\frac{\partial P}{\partial X}+\frac{1}{\mathrm{Re}}\left(\frac{\partial^2 U}{\partial X^2}+\frac{\partial^2 U}{\partial Y^2}\right)\ , \tag{3}$$

$$\frac{\partial V}{\partial \tau}+U\frac{\partial V}{\partial X}+(V-\hat{V})\frac{\partial V}{\partial Y}=-\frac{\partial P}{\partial Y}+\frac{1}{\mathrm{Re}}\left(\frac{\partial^2 V}{\partial X^2}+\frac{\partial^2 V}{\partial Y^2}\right)\ , \tag{4}$$

Energy equation

$$\frac{\partial \theta}{\partial \tau}+U\frac{\partial \theta}{\partial X}+(V-\hat{V})\frac{\partial \theta}{\partial Y}=\frac{1}{\mathrm{Pr\ Re}}\left(\frac{\partial^2 \theta}{\partial X^2}+\frac{\partial^2 \theta}{\partial Y^2}\right)\ . \tag{5}$$

As the time $\tau>0$, the boundary conditions are as follows:

On the fluid inlet surface AB

$$U=1,\quad V=0,\quad \theta=0\ , \tag{6}$$

On the wall surfaces of the channel BC and AD

$$U=V=0,\quad \partial\theta/\partial Y=0\ , \tag{7}$$

On the fluid outlet surface CD

$$\frac{\partial U}{\partial X}=\frac{\partial V}{\partial X}=\frac{\partial \theta}{\partial X}=0\ , \tag{8}$$

On the interfaces between the fluid and fins

$$U=0,\quad V=V_f,\quad \theta=1\ . \tag{9}$$

## 3 Numerical method

A Galerkin finite element method and a backward scheme to deal with the time terms are utilized to discretize the governing equations and boundary conditions. The Newton–Raphson iteration algorithm and the penalty function model [15] are utilized to simplify the nonlinear and pressure terms, respectively, in the momentum equations. The velocity and temperature terms are approximated by quadrilateral and nine-node quadratic isoparametric elements. The discretization processes of the governing equations are similar to the one used in [16]. The details of the numerical method and solution procedures are delineated in [13, 14].

The relative errors of each variable to examine the convergence criteria are defined as follows:

$$\left|\frac{\phi^{m+1}-\phi^m}{\phi^{m+1}}\right|_{\tau+\Delta\tau}<1.0\times10^{-3},\quad \text{where } \phi=U,V,\theta\ . \tag{10}$$

Besides, the conservative residual of the continuity equation is checked for each element on each time to ensure the mass conservative law to be satisfied. In the computing process of this study, the residual of the continuity equation for element is smaller than $1.0\times10^{-7}$.

## 4 Results and discussion

The dimensionless geometric lengths are listed in Table 1. The working fluid is air with $\mathrm{Pr}=0.71$ and Reynolds numbers are equal to 500 and 1000. Several different swinging speeds $S_f$ $(S_f=s_f/u_0=|V_f|)$ and swinging amplitudes $A(=a/w_2)$ of the fins are taken into consideration.

Since the thickness of the fins $H_3=0.01$ is very thin, the heat transfer from the right and left surfaces of the fins can be neglected. The local Nusselt numbers on the top and bottom surfaces of the fin are defined by

$$\mathrm{Nu}_X(X,\tau)=-\frac{\partial\theta}{\partial Y}\ . \tag{11}$$

The average Nusselt numbers on the top and bottom surfaces of the fin are defined as

$$\overline{\mathrm{Nu}_X}(\tau)=\frac{1}{W_2}\int_0^{W_2}\mathrm{Nu}_X\,dX\ , \tag{12}$$

where $W_2$ is the length of the fin. In addition, the overall average Nusselt number of the fin is defined as

**Table 1.** The dimensionless geometric parameters

| $H$ | $H_1$ | $H_2$ | $H_3$ | $W$ | $W_1$ | $W_2$ | $W_3$ |
|---|---|---|---|---|---|---|---|
| 7.0 | 3.085 | 0.4 | 0.01 | 15.0 | 4.0 | 1.0 | 10.0 |

$$\mathrm{Nu}(\tau) = \frac{1}{2W_2} \times \left( \int_0^{W_2} \mathrm{Nu}_X \Big|_{\substack{\text{top} \\ \text{surface}}} \mathrm{d}X + \int_0^{W_2} \mathrm{Nu}_X \Big|_{\substack{\text{bottom} \\ \text{surface}}} \mathrm{d}X \right) \tag{13}$$

Integration of the overall average Nusselt number over time of one cycle of the motion of swinging back and forth leads to the time-average overall Nusselt number on the fin



$$\overline{\mathrm{Nu}} = \frac{1}{\tau_\mathrm{p}} \int_0^{\tau_\mathrm{p}} \mathrm{Nu}\, \mathrm{d}\tau \ , \tag{14}$$

where $\tau_\mathrm{p}$ is the time of one cycle of the swinging of the fins.

To ensure the accuracy of computational results, a series of numerical tests for various meshes at the steady state are carried out. The nonuniform distribution of 3872 elements corresponding to 15,942 nodes is chosen. Since the pitch of the fins ($H_2 = 0.4$) is much larger than the thickness of the fins ($H_3 = 0.01$), the flow and thermal fields at the steady state are similar to the fluid flowing over a flat plate. The Blasius solution [17] for the average Nusselt number with laminar flow over a flat plate with length $\iota$ is expressed by

$$\overline{\mathrm{Nu}_X} = 0.664\, \mathrm{Re}_\iota^{1/2} \mathrm{Pr}^{1/3} \ . \tag{15}$$

The average Nusselt number on the top or bottom surface of the middle fin at the steady state for different Reynolds numbers compared with those of the Blasius solutions are tabulated in Table 2. The largest difference of only 1.8% in the average Nusselt number was found between the present study and Blasius solutions. As for the selection of the time step $\Delta\tau$, the time step $\Delta\tau = 1.0 \times 10^{-2}$, $5.0 \times 10^{-3}$ and $2.5 \times 10^{-3}$ are chosen for the swinging speed of the fins $S_\mathrm{f} = 0.05$, 0.5 and 1.0 cases, respectively.

For clearly indicating the variations of the flow and thermal fields, the velocity vectors and isothermal lines around the middle fin are only presented. However, it should be noted the computational domain included three swinging fins, and a much larger region was calculated than what is displayed in the subsequent figures. Besides, the velocity vectors shown in the following figures are scaled relatively to the maximum velocity in the flow field.

The transient developments of the velocity vectors and isothermal lines around the middle fin for the swinging speed of the fins $S_\mathrm{f} = 0.05$ and the amplitude of the fins $A = 0.05$ under $\mathrm{Re} = 500$ case are shown in Fig. 2. At the time $\tau = 0.0$ (Fig. 2a), the fins are stationary and the fluid flows steadily. As the time $\tau > 0$, the fins begin to swing back and forth. As shown in Fig. 2b, the fin is on the way to move upward. The fin pushes the fluid near the top surface of the fin, which enhances the heat transfer near the top surface of the fin. In the meantime, the fluid near the bottom surface of the fin replenishes the vacant space near the bottom surface of the fin induced by the movement of the fin. Most of the fluid near the bottom surface of the fin are difficult to catch up to the bottom surface of the fin in time, which is disadvantageous to the heat transfer. Afterwards, the fin moves upward continuously until the amplitude of the fin $A$ is equal to 0.05. The variations of the flow fields are similar to those mentioned above.

**Table 2.** Comparison of the average Nusselt number of the middle fin at the steady state for different Reynolds numbers of the present study with the Blasius solution

| | Re | | | |
|---|---|---|---|---|
| | 100 | 500 | 1000 | 1500 |
| Blasius solution | 5.92 | 13.25 | 18.73 | 22.94 |
| Authers' results | 5.97 | 13.57 | 18.70 | 22.52 |

The fin turns downward immediately as the fin reaches the maximum upper amplitude. As shown in Fig. 2c, the fin is on the way to move downward and the position of the middle fin is at the center of the channel. The variations of the flow fields are opposite to those of the upward movement of the fin mentioned earlier. The fin pushes the fluid near the bottom surface of the fin and the fluid close to the top surface of the fin continuously replenishes the vacant space near the top surface of the fin.

In Fig. 2d, the fin is on the way to move upward and the position of the middle fin returns to the center of the channel. The variations of the flow fields are similar to those as shown in Fig. 2b. As the time increases, the fins swing back and forth as mentioned above. Since the swinging speed of the fins is slow, the variations of the flow fields are slight.

As for the thermal fields, the variations of the thermal fields usually correspond to the variations of the flow fields. Since the fins swing with a small speed, the flow fields are similar to the fluid flowing over a flat plate. Thus, the variations of the thermal fields are slight and the distributions of the isothermal lines are similar to those of the fluid flowing through a flat plate.

Figure 3 shows the time variations of the average Nusselt number on the top and bottom surfaces of the middle fin at the same conditions as shown in Fig. 2. Based upon the variations of the flow and thermal fields mentioned earlier, as the fin moves upward, the average Nusselt number increases on the top surface of the fin and decreases on the bottom surface of the fin. As the fin moves downward, the results of the variations of the average Nusselt number on the surface of the fin are opposite to those of the fin moving upward. Furthermore, as shown in Fig. 4, the variations of the time-average overall Nusselt number on the middle fin with time compared with those of the steady state are very slight.

In Fig. 5, there are the transient developments of the velocity vectors and isothermal lines around the middle fin for the swinging speed of the fins $S_\mathrm{f} = 0.5$ and the amplitude of the fins $A = 0.05$ under $\mathrm{Re} = 500$ case. Since the swinging speed of the fins is greater than that of the case above, the variations of the flow and thermal fields around the fins are more drastic than those of the case above. At the beginning of the motion, as shown in Fig. 5b, the fin is on the way to move upward. The fluid near the top surface on the fin is pushed by the fin and flows upward. Conversely, the fluid close to the left and bottom surfaces of the fin simultaneously replenishes the vacant space

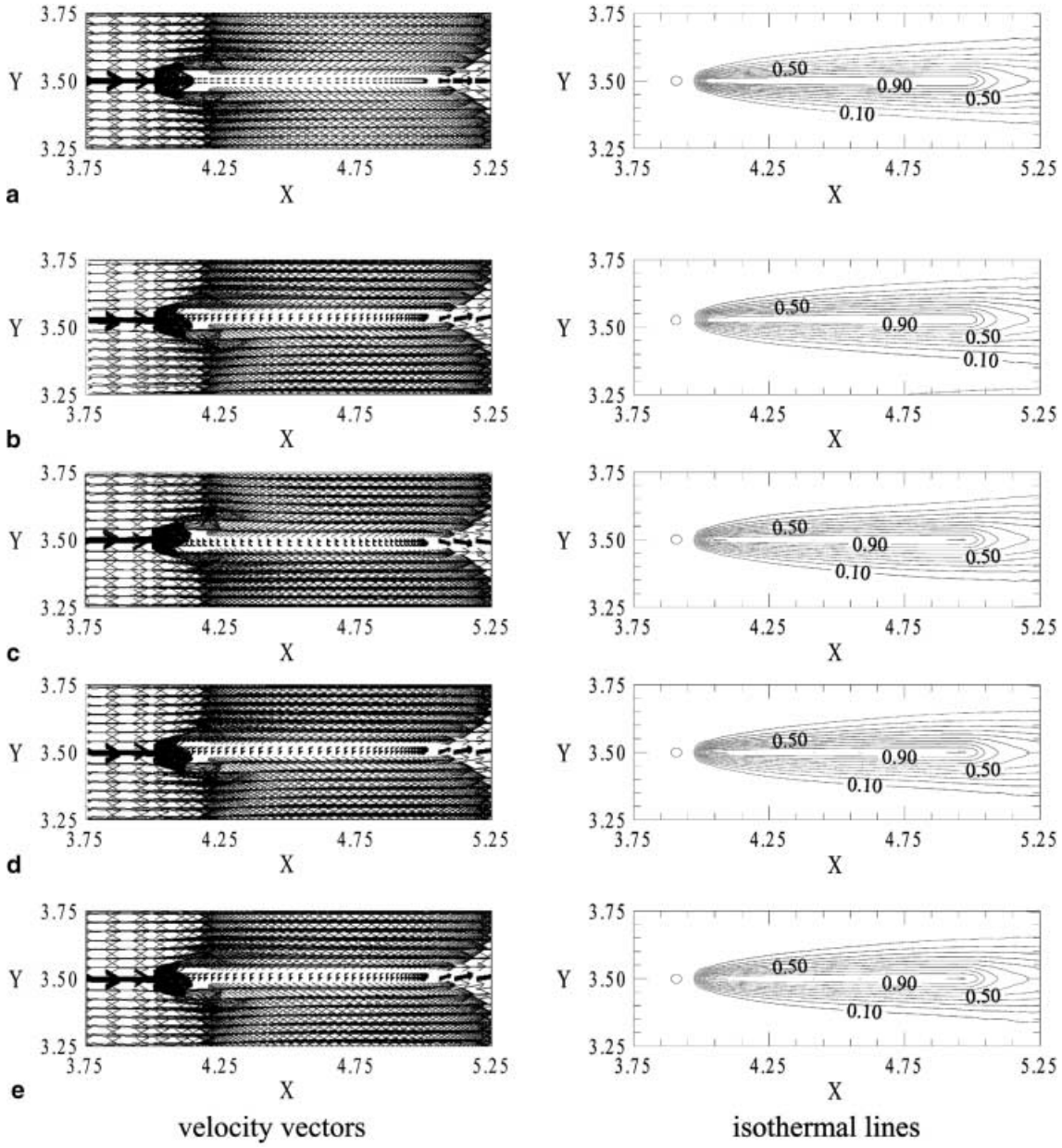


**Fig. 2a–e.** The transient developments of the velocity vectors and isothermal lines around the middle fin for the $S_f = 0.05$, $A = 0.05$ and $Re = 500$ case **a** $\tau = 0.0$, **b** $\tau = 0.6$, **c** $\tau = 2.0$, **d** $\tau = 4.0$, **e** $\tau = 20.0$

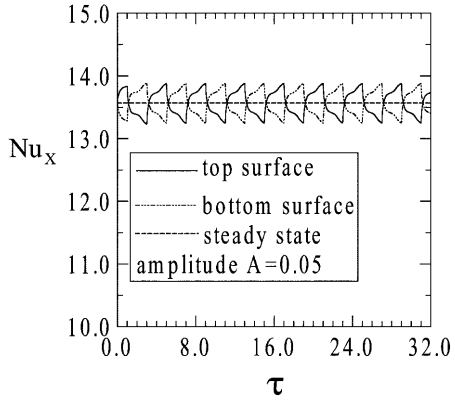


**Fig. 3.** The variations of the average Nusselt number on surfaces of the middle fin with time for the $S_f = 0.05$ and $Re = 500$ case

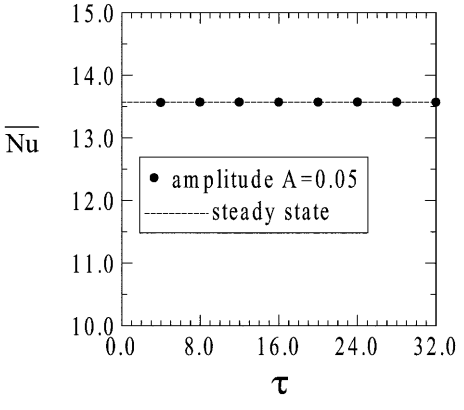


**Fig. 4.** The variations of the time-average overall Nusselt number on the middle fin with time for the $S_f = 0.05$ and $Re = 500$ case

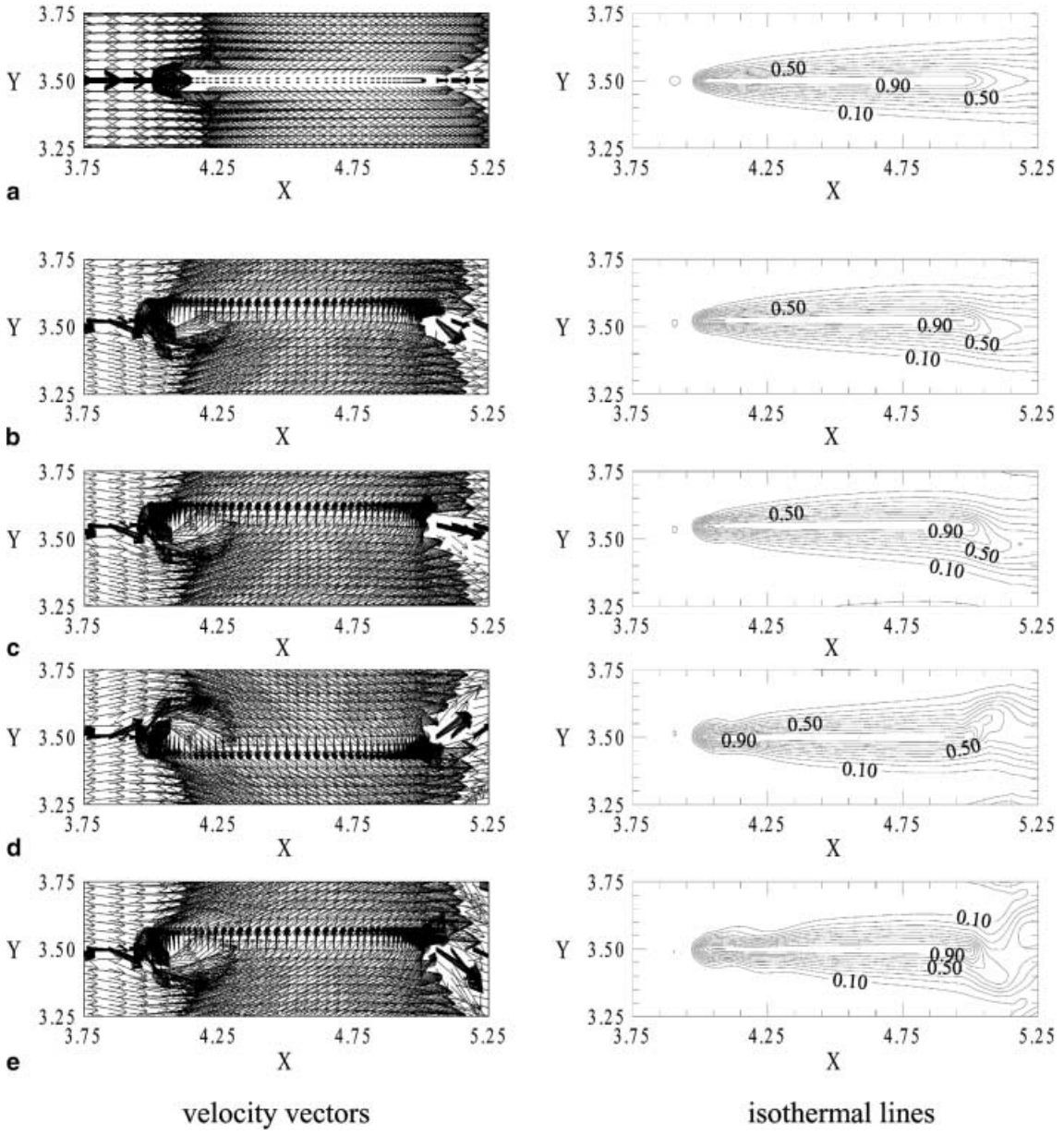


**Fig. 5a–e.** The transient developments of the velocity vectors and isothermal lines around the middle fin for the $S_f = 0.5$, $A = 0.05$ and $Re = 500$ case **a** $\tau = 0.0$, **b** $\tau = 0.05$, **c** $\tau = 0.1$, **d** $\tau = 0.2$, **e** $\tau = 0.4$

induced by the movement of the fin near the bottom surface of the fin. Consequently, a small recirculation zone, which is disadvantageous to the heat transfer, is observed around the left corner of the bottom surface of the fin. The variations of the isothermal lines are slight at this time.

As the time increases, the fins move upward continuously as indicated in Fig. 5c. The flow and thermal fields are similar to those mentioned earlier, but the recirculation zone around the left corner of the bottom surface of the fin enlarges gradually.

As shown in Fig. 5d, the fin is on the way to move downward and the position of the middle fin is at the center of the channel. Due to the downward movement of the fin, the fin pushes the fluid near the bottom surface of the fin, and the fluid near the left and top surfaces of the fin simultaneously replenishes the vacant space near the top surface of the fin. As a result, a recirculation zone is formed around the left corner of the top surface of the fin.

As the time increases (Fig. 5e–j), since the fin is in motion of swinging back and forth with a large swinging speed, the recirculation zones and reattachment flows around the top and bottom surfaces of the fin are formed alternately and continuously, and migrate to the downstream gradually. As a result, the variations of isothermal lines are like a wavy motion. These could cause the boundary layers of the flow and thermal fields to be contracted and disturbed during the transient developments, which enhance the heat transfer of the fin. The distributions of the isothermal lines become sparser near the recirculation zones and denser near reattachement flows.

Figure 6 indicates the time variations of the time-average overall Nusselt number on the surface of the

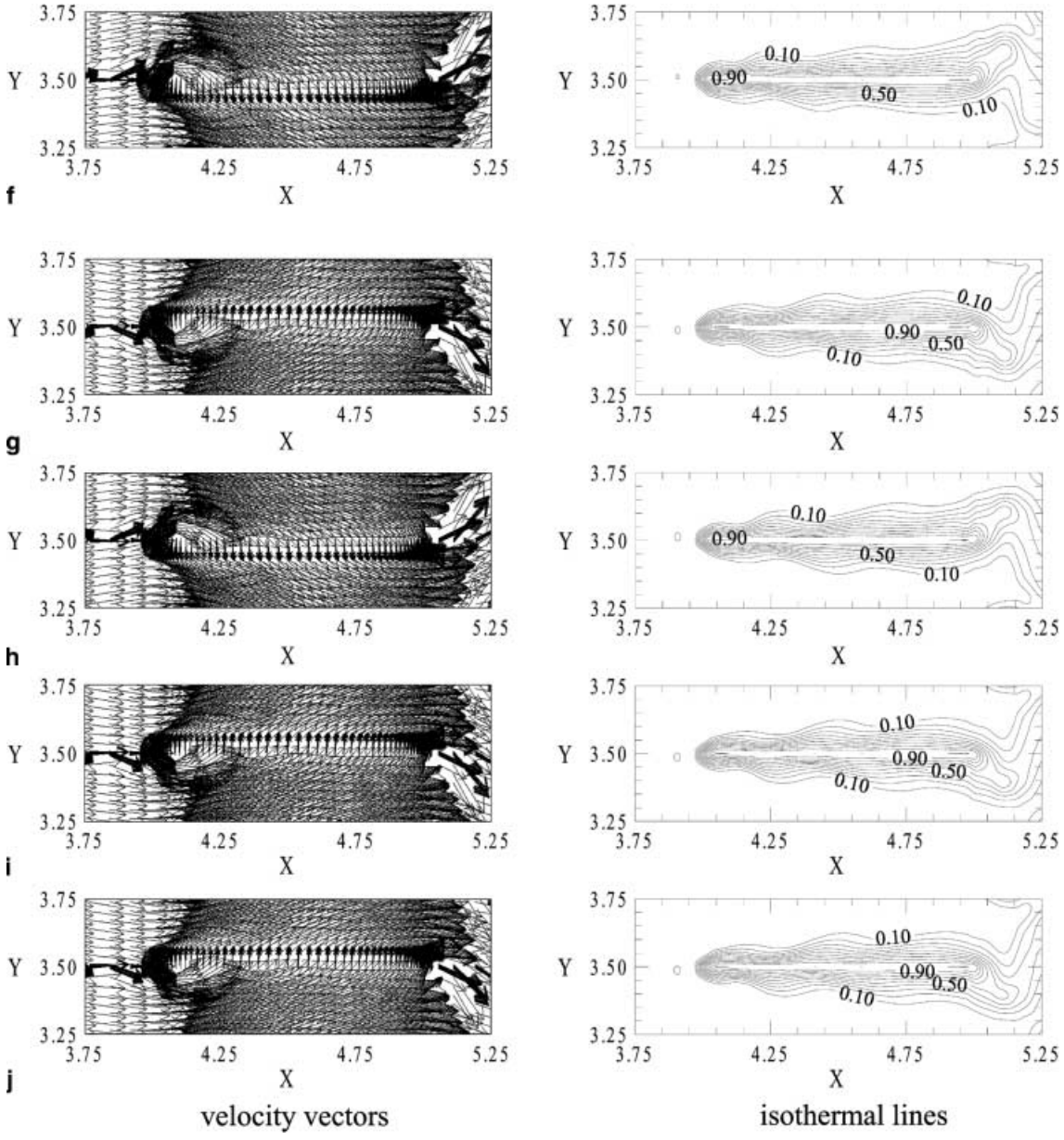


**Fig. 5f–j.** The transient developments of the velocity vectors and isothermal lines around the middle fin for the $S_f = 0.5$, $A = 0.05$ and Re = 500 case **f** $\tau = 1.0$, **g** $\tau = 2.0$, **h** $\tau = 3.8$, **i** $\tau = 4.0$, **j** $\tau = 8.0$

middle fin at the same conditions as shown in Fig. 5. Based upon these reasons mentioned above, the time-average overall Nusselt number during the transient developments is enhanced. Furthermore, the flow and thermal fields may approach a stable state as the time increases, and the mean increment of the time-average overall Nusselt number on the middle fin is about 10% in the computing range. As expected, the heat transfer rate increases with increased the swinging speed of the fins. Moreover, the mean increment of the time-average overall Nusselt number for the amplitude of the fins $A = 0.1$ case is about 16%, which is larger than that of the $A = 0.05$ case.

Figure 7 shows the time variations of the time-average overall Nusselt number on the middle fin for the swinging speed of the fins $S_f = 1.0$ and Re = 500 under the amplitude of the fins $A = 0.05$, 0.1 and 0.15 cases. In the

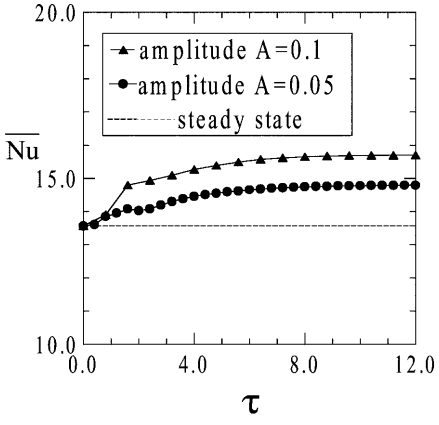


**Fig. 6.** The variations of the time-average overall Nusselt number on the middle fin with time for the $S_f = 0.5$ and Re = 500 case

computing range, the mean increments of the time-average overall Nusselt number are about 18, 37 and 38% corresponding to the amplitudes of the fins $A = 0.05$, 0.1 and 0.15 cases, respectively. The results show that the heat transfer is enhanced significantly as the amplitude of the fins increases from 0.05 to 0.1. But, as the amplitude of the fins increases from 0.1 to 0.15, the enhancement of the heat transfer is slight, this could be that the flow and thermal fields had approached an optimal condition.

The time variations of the time-average overall Nusselt number on the middle fin for the swinging speed of the fins $S_f = 0.5$ and the amplitude of the fins $A = 0.05$ under $Re = 1000$ case is indicated in Fig. 8. As the time increases, the flow and thermal fields may approach a stable state and vary slightly. In the computing range, the mean increment of the time-average overall Nusselt number on the middle fin is about 15%.

Figure 9 shows the time variations of the time-average overall Nusselt number on the middle fin for the swinging speed of the fins $S_f = 1.0$ and $Re = 1000$ under the amplitude of the fins $A = 0.05$ and 0.1 cases. The variations of the time-average overall Nusselt number with time are hardly found out to approach a stable state, this is suggested as that the swinging speed of the fin is too fast and

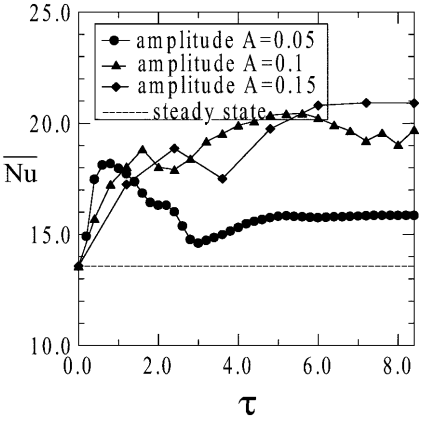


**Fig. 7.** The variations of the time-average overall Nusselt number on the middle fin with time for the $S_f = 1.0$ and $Re = 500$ case

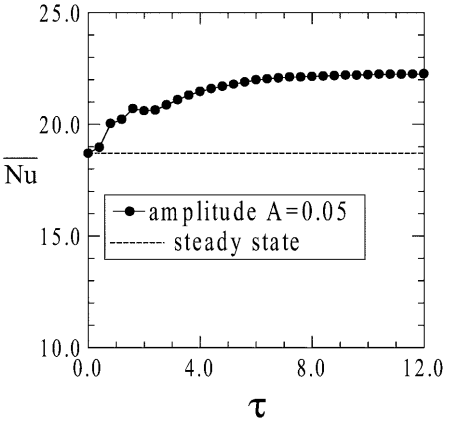


**Fig. 8.** The variations of the time-average overall Nusselt number on the middle fin with time for the $S_f = 0.5$ and $Re = 1000$ case

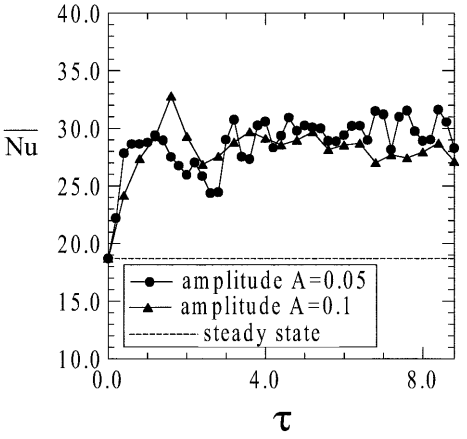


**Fig. 9.** The variations of the time-average overall Nusselt number on the middle fin with time for the $S_f = 1.0$ and $Re = 1000$ case

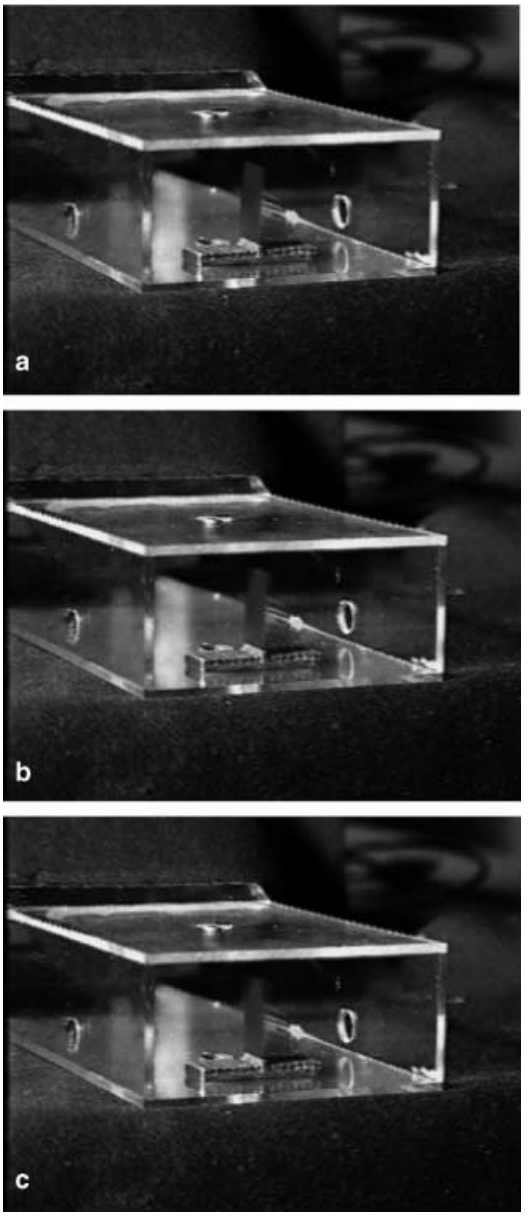


**Fig. 10a–c.** The photograph of the swinging of the fin in **a** stationary, **b** and **c** swinging

the flow and thermal fields are unable to develop regular patterns in time. In the computing range, the mean increments of the time-average overall Nusselt number on the middle fin are about 54 and 52% for $A = 0.05$ and 0.1 cases, respectively.

## 5 Conclusions

The heat transfer of extremely thin fins of a finned heat sink swinging back and forth in a flow is investigated numerically. Some conclusions are summarized as follows:

1. As the fins swing with a relatively low speed, the variations of the flow and thermal fields may approach to regular patterns with time. However, the variations of the flow and thermal fields are unable to develop regular patterns with time as the fins swing with a large speed.
2. As the fins swing with a large speed, the recirculation zones and reattachement flows are observed around the fins alternately and continuously, and migrate to the downstream gradually. This may cause the velocity and thermal boundary layers to be contracted and disturbed, which results in a significant enhancement of the heat transfer.
3. The swinging amplitude of the fins affects the enhancement of heat transfer remarkably.

## Appendix

The photographs of the swinging of the fin induced by a flow are shown in Fig. 10. A finned heated sink with single extremely thin fin is set on the test section of a small wind tunnel. The extremely thin fin is made of Co-based amorphous ribbon and 25 μm in thickness. As shown in Fig. 10a, both the fluid and fin are stationary. In Fig. 10b–c, the fluid flows through the tunnel. The extremely thin fin is then swinging induced by the flow. Thus, the images of the fin in the photographs are foggy.

## References


1. **Incropera FP** (1988) Convection heat transfer in electronic equipment cooling. J Heat Transf 110: 1097–1111
2. **Yeh LT** (1995) Review of heat transfer technologies in electronic equipment. J Electro Packaging 117: 333–339
3. **Sathe S; Sammakia B** (1998) A review of recent developments in some practical aspects of air-cooled electronic packages. J Heat Transf 120: 830–839
4. **Markstein HW** (1975) New development in cooling techniques. Electro Packaging and Production 16: 36–44
5. **Sathe S; Karki KM; Tai C; Lamb C; Patanker SV** (1997) Numerical prediction of flow and heat transfer in an impingement heat sink. J Electron Packaging 119: 58–63
6. **Vafai K; Lu Z** (1999) Analysis of two-layered micro-channel heat sink concept in electronic cooling. Int J Heat Mass Transf 42: 2287–2297
7. **Saxena UC; Laird ADK** (1978) Heat transfer from a cylinder oscillating in a cross-flow. J Heat Transf 100: 684–689
8. **Kurzweg UH** (1988) Heat transport along an oscillating flat plate. J Heat Transf 110: 789–790
9. **Cheng CH; Hong JL; Aung W** (1997) Numerical prediction of lock-on effect on convective heat transfer from a transversely oscillating circular cylinder. Int J Heat Mass Transf 40: 1825–1834
10. **Cheng CH; Chen HN; Aung W** (1997) Experimental study of the effect of transverse oscillation on convection heat transfer from a circular cylinder. J Heat Transf 119: 474–482
11. **Hughes TJR; Liu WK; Zimmermann TK** (1981) Lagrangian–Eulerian finite element formulation for incompressible viscous flows. Comput Meth Appl Mech Eng 29: 329–349
12. **Donea J; Giuliani S; Halleux JP** (1982) An arbitrary Lagrangian–Eulerian finite element method for transient dynamic fluid–structure interactions. Comput Meth Appl Mech Eng 33: 689–723
13. **Fu WS; Yang SJ** (2000) Numerical simulation of heat transfer induced by a body moving in the same direction as flowing fluids. Heat Mass Transf 36: 257–264
14. **Fu WS; Yang SJ** (2001) Heat transfer induced by a body moving in opposition to a flowing fluid. Int J Heat Mass Transf 44: 89–98
15. **Reddy JN; Gartling DK** (1994) The finite element method in heat transfer and fluid dynamics. CRC Press, Inc., ch. 4
16. **Fu WS; Kau TM; Shieh WJ** (1990) Transient laminar natural convection in an enclosure from steady flow state to stationary state. Numer Heat Transf A 18: 189–211
17. **Incropera FP; Dewitt DP** (1990) Fundamentals of heat and mass transfer. John Wiley & Sons, ch. 7